Nigerian Journal of Physics (NJP)
ISSN online: 3027-0936
ISSN print: 1595-0611
DOI: https://doi.org/10.62292/njp.v34i4.2025.408
Volume 34(4), December 2025

The Impact of Fe-Doping on the Structural, Optical and Electric Properties of MnO_2 Thin Films Prepared by Spray Pyrolysis Technique for Solar Application

[1]Medina Umar, [2]Adeoye Abiodun Eyitayo and [1]Salaudeen Olaiya Abdulwasiu

[1]Department of Physics, Faculty of Science, University of Abuja, Gwagwalada FCT Abuja
[2]Department of Physics and Science Laboratory Technology, Faculty of Science, First Technical University Ibadan, Ibadan

*Corresponding Author's Email: medina.umar@uniabuja.edu.ng

ABSTRACT
Pure and Fe-doped MnO_2 was deposited at different atomic concentration of 2, 4, 6, and 8% in this research work on a glass slide substrate using the spray pyrolysis deposition technique. The nanoparticle was then characterized in other to obtain its structural, optical, chemical composition and electrical properties. The X-ray analysis reveal the crystal nature of the thin film nanoparticles, the optical properties of the nanoparticle were obtained from the UV-Vis spectroscopy, where the absorbance and the energy band gap of the nanostructures was determined. The FTIR characterization gives the chemical composition of the thin film which falls within the manganese oxide vibration range, and the hall effect data gives the resistivity, conductivity and the mobility of the charge carriers. The resistivity first decreases then increase as a result of the dopant, the exponential value of the resistivity was found to be $10^4 \Omega$cm which agrees with the required value for buffer layer of photovoltaic cell.

Keywords:
Manganese Oxide,
Spray Pyrolysis,
Hall Effect,
UV-Vis Spectroscopy,
XRD,
FTIR.

INTRODUCTION

Nanostructures are highly considered to be significant in the advancement of technology, the properties of many nanostructures has been reported such as ZnS, CuO, CdS, etc. doping with several element such as Zn, Fe, Mg and so on in other to improved it properties for device application Zahan and Podder (2020) and Liu et al (2022) Recently, metal oxide (Zinc oxide, manganese oxide, copper oxide etcetera) has been examined through which it electrical, chemical, magnetic and optical properties where observed. The general properties of the metal oxide are easily obtained because of their oxygen rich which makes them environmentally friend during fabrication Sasikala, Varshaa and Kalaiselvi (2020) and Umar et al (2021). Manganese dioxide (MnO_2) with oxidation number of +4 reported by Hastuti, Subhan, Amonpattaratkit, Zainuria and Suasmoro (2021) and (Dakhel, 2008) is an N-Type semiconductor with electron as charge carriers Nassiri, Hadri, Chafi, El Hat, Hassanain, Rouchdi, Fares and Mzerd (2017). it is widely studied with some atomic doping percentage of metals in other to improve it optical, electrical chemical and magnetic properties studied by Liang, Chen, Xu, Wang, Zhou and Yan, (2023) and Gokon, Nishizawa, Yawata, Bellan, Kodama and Cho (2019). The energy band gap of MnO_2 nanostructures has been experimentally reported to be at the range of 2.5 - 3.5 eV with crystalline size of 10-50nm observed by Song, Duan, Cui and Huang (2022). doping it with metals further improved it performances which is highly recommendable for solar, sensors, medical, capacitors and thermal applications etcetera. A typical solar cell is made up of different phases, such as the front contact made of n-type semiconductor, the absorption layer and the back contact made of p-type semiconductor. For the purpose of solar cell application MnO_2 is doped with different metals in other to make it suitable for solar application. Iron (Fe) is a transitional metal with many oxidations states such as Fe^{2+}, Fe^{3+} and so on, as it is observed in different compound (Hazaa, 2013). Due to the significant electrical properties of Fe, doping Fe with manganese oxide with naturally and chemical improved the properties of the thin film and as well reduce it energy band gap Clark and Marsden (2024) and Silver (1993). The different method has been deployed for the deposition of manganese oxide nanostructures, some of the common methods used include chemical precipitation Sasikala et al. 2020. Spray pyrolysis technique (Dakhel, 2008) and Yadav, Shukla and Sharma (2022), Liang et al (2023) worked on thermos-gravimetric reactor, hydrothermal method, chemical deposition method by Mane and Lokhande (2000) and Levish, Joshi and Winterer (2023). The spray pyrolysis deposition technique is now commonly used for the deposition of thin film nanostructures because it is cheap, simple to set up and environmentally friendly which makes it highly compactible for manganese oxide deposition due to the presence of abundance oxygen.

This research is focus on depositing pure MnO_2 nanoparticles on a glass substrate doping it with Fe at different atomic concentrations using the spray pyrolysis deposition technique, where the structural, optical and electric properties of the thin film will be determined in other to find its usefulness in solar cells.

MATERIALS AND METHODS

The cleansing process of the glass substrates was rigorous in other to make sure that it is impurity disinfected, the beakers and the forceps were also well washed with distilled water and was allowed to dry. 150ml of Ethanol was placed inside the beakers where the impurity free forceps was used to pick the glass substrates and was placed in the beaker containing the ethanol, it was allowed to remain inside the beaker for 60minutes. Manganese Chloride Tetra-hydrates ($MnCl_2.4H_2O$) was used as the precursor for pure MnO_2, 0.1M of the manganese Chloride tetra-hydrate was dissolved in 250ml diluted water and magnetic stirrer was used to stir the solution for 40min at 0^0C, the forceps was used to pick the glass slide rinsed with distilled water and place on a hot plate reading 350^0C in an oven. The prepared manganese oxide was then sprayed on the glass substrate in an oscillatory form at a distance of 55cm at an angle of 60^0 with 10min breakdown for rest to avoid temperature fluctuation. The doping concentration was done by similarly dissolving 0.1M of Iron Chloride Tetra-hydrate ($FeCl_2.4H_2O$) in 250ml of diluted water, and the MnO_2 solution was doped with Fe in atomic concentration of 2, 4, 6, and 8%. When the spray was completed, the forceps was used to pick the thin film nanoparticles deposited and kept in a hot furnace for 10min, after which it was cooled and then taken for UV, XRD, FTIR and Hall Effect characterization, the color of the first sample from right is champagne gold while the rest remain dark brown.

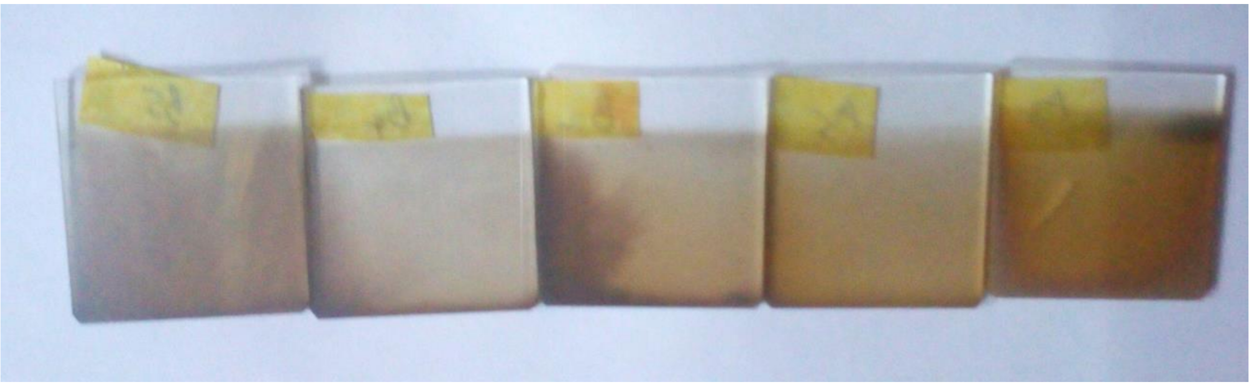

Plate 1: Glass Substrate of Thin Film Nanoparticles

In other to determine the structural properties of the thin film nanoparticles, the X-ray diffraction technique was used with $K\alpha$ = 1.5Å of Cu, the X-ray diffractometer thermos scientific model (ARL'XTRA X-Ray:197492086) was used to collect the XRD data at 2θ (3-70^0) range. The optical properties of the nanostructures was obtain using the UV-Vis Spectrometer (Filmetric F10-RT), at wavelength of 190-1200nm range, from where the absorbance, reflectance, transmittance and the energy gab was determined. The electrical properties of the thin film nanostructures was determined using the HMS3000, which result to obtaining the resistivity, conductivity and the mobility of the nanostructures. The FTIR characterization was used to obtain the chemical formation of the thin film, it was done at a wavelength ranging from 400-4000cm^{-1}.

RESULTS AND DISCUSSION

X-Ray Diffraction (XRD) Properties

The X-ray diffraction characterization was carried for all the nanoparticles thin film (pure MnO_2 2% 4% 6% and 8%) at 2θ ranging from 3-700. The intensity of the nanoparticles was affected by the level of doping concentration which increases significantly across diffraction angle. Figure 2.0 show the XRD pattern of the nanoparticle, it was observed that the XRD peaks matched with each other at 100, 002, 101, 102, 110, 103 and 112 crystallographic plane at 2θ = 32.020, 34.670, 36.470, 47.80, 56.920, 62.940 and 67.950 respectively. The peaks sharpness confirm the crystal nature of the nanoparticles at different concentration of Fe doping.

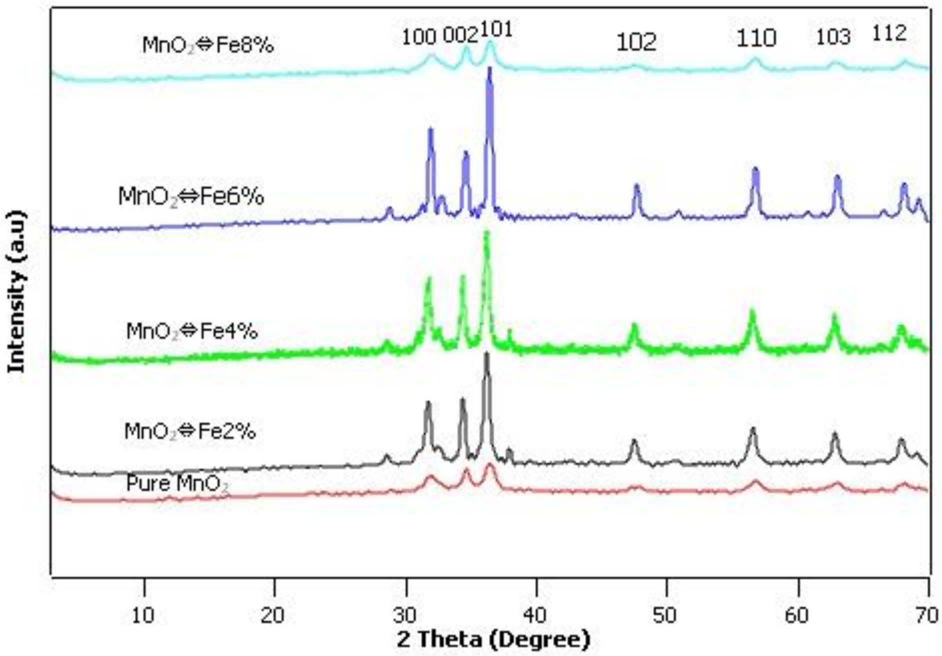

Figure 1: XRD Characterization of the thin film nanoparticles

The lattice constant parameter of the thin film nanoparticles was calculated using the interplanar spacing relation as shown:

$$\frac{1}{d_{hkl}} = \frac{h^2+k^2}{a^2} + \frac{l^2}{c^2} \quad (1)$$

Where d_{hkl} represent the interplanar spacing of the nanoparticles, h, k and l represent the planes of the thin film while a=b and c (Julien and Mauger, 2017 and Sahel 2023) represent the lattice constant parameter for a tetragonal structural material. d_{hkl} of the thin film was calculated using Bragg's law relation given as follows;

$$n\lambda = 2d_{hkl}\sin\theta \quad (2)$$

Where n is the diffraction order of the thin film, λ is the wavelength of the XRD data given as 1.5406Å for CuKa, and θ is the Bragg's angle in degrees as seen in Patrice, Dupont, Jumas, Wang and Tarascon (2004).

Table 1: Bragg's angle, Full Width half Maximum, hkl and interplanar spacing of the thin film

θ	*β*	*hkl*	d_{hkl}
15.515	0.44	100	2.8797
17.2515	0.316	002^{c}	2.5974
18.136	0.472	101	2.4747
23.775	0.16	102	1.9107
28.32	0.44	$110^{a=c}$	1.6237
31.3915	0.74	103	1.4788
33.925	0.49	112	1.3802

Table 1 shows the Braggs angle, the full with half maximum, hkl and the interplanar spacing of the thin film nanostructures. The lattice constant was calculated is presented in Table 2 for a=b and c which confirmed the tetragonal nature of Fe-doped MnO_2, and the unit volume (V) of the thin film nanoparticles in Yadav, Shukla and Sharma (2022) and Vijaykumar, Manjunatha and Sannakki (2024). The crystal size (D) of the nanoparticles were also calculated from the XRD data using the Debye-Scherer equation below;

$$D = \frac{k\lambda}{\beta cos\theta} \quad (3)$$

Where D (nm) represent the crystalline size of the thin film nanoparticle, k is the Scherer Constant which is 0.94, λ is the XRD wavelength and for CuKa λ=1.5406Å, β is the full width half maximum (FWHM) and θ is the Bragg's angle as shown in Table 2.

Table 2: XRD data analysis for Fe-doped MnO2 nanostructures

Samples	a=b (Å)	c (Å)	V ($Å^3$)	δ x 10^{-3}	D (nm)	ε x 10^{-3}
Pure MnO_2	2.2963	5.1948	10.4678	2.0141	22.2824	2.400
MnO_2 ⇔ *Fe2%*	2.2860	5.1705	10.3963	1.1779	9.2139	-0.7720
MnO_2 ⇔ *Fe4%*	2.2963	5.1948	10.4678	1.6565	24.5703	1.6545
MnO_2 ⇔ *Fe6%*	2.2900	5.1697	10.4138	1.2588	28.1857	0.0228
MnO_2 ⇔ *Fe8%*	2.2852	5.1633	10.3854	1.1090	9.4958	0.0119

The crystal size (D) nm revealed by Radhamani, Surendra and Rao, (2018) and Khan, Mohammad, Mohammad, Tariq, Khan, Hussain, Aktar and Rahamn, (2019), the thin film was not significantly affected by the Fe doping concentration, the crystal size first decreases and increases down the doping percentage as shown in figure 1. The dislocation density (δ) of the thin film nanoparticles where obtained from the equation below;

$$\delta = \frac{1}{D^2} \quad (4)$$

The dislocation density δ of the nanostructure was high for the pure MnO_2, but there was no specific pattern of the doping concentration effect on δ as it decreases across the Table. Similarly the tensile strain (ε) of the nanostructures was obtained from the relation below;

$$\beta_T = \beta_D + \beta_\varepsilon \quad (5)$$

Where β_T represent absolute broadening of the thin film, β_D is the crystal size of the nanostructure and βε is the tensile strain broadening of the nanoparticle. A linear fitting was used to obtain the tensile strain of the nanoparticle using the Williams-Hall Plot analysis, a compression strain of – 0.7720 was observed at the MnO_2 ⇔ *Fe 2*% thin film.

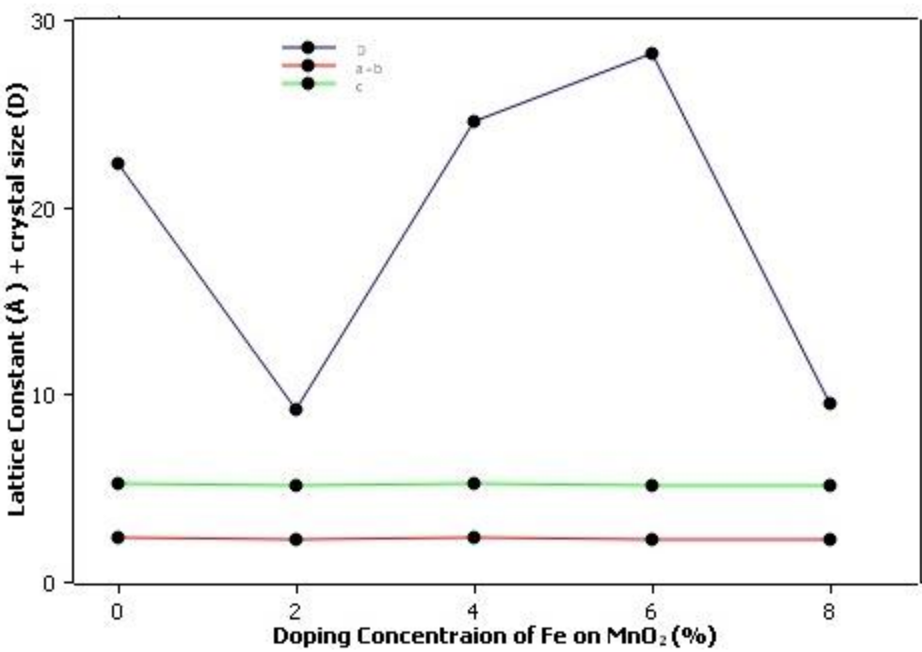

Figure 2: Identifying significant changes of the doping concentration on D (nm) and a=b, c (Å)

Optical Analysis of Fe-Doped MnO_2 Thin Film Nanostructures

The UV-Vis spectrometer was used to obtain the optical characterization of the nanostructures, Absorbance, Transmittance, Reflectance and the energy band gap was determined from the data generated from the UV spectroscopy analysis at wavelength ranging from 190-1200nm. Figure 3 shows the absorbance spectrum of the thin film nanostructures, the absorbance of the thin film was absorbed at 300.5nm and becomes more effective with increase in Wavelength. Figure 4 shows the Reflectance Spectrum of the thin film nanostructures, the reflectance was found around 3.28-9.78%. The thin film nanostructure shows desirable reflectance properties which is highly recommendable for device application

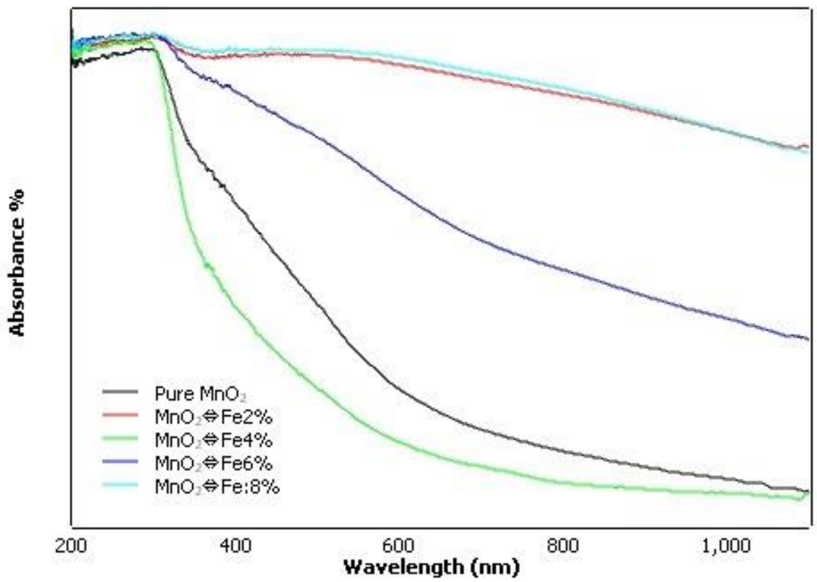

Figure 3: Absorbance Spectrum of the Fe-doped MnO2 Thin Film Nanostructures

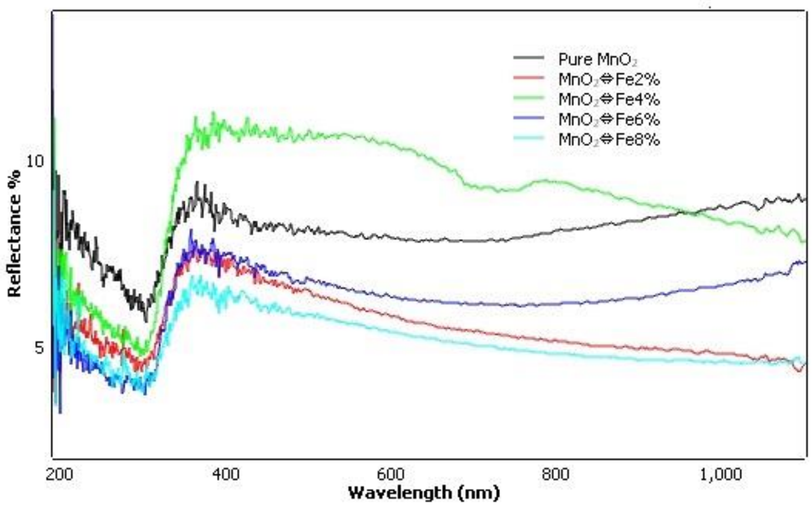

Figure 4: Reflectance Spectrum of Fe-doped MnO2 Thin Film nanostructures

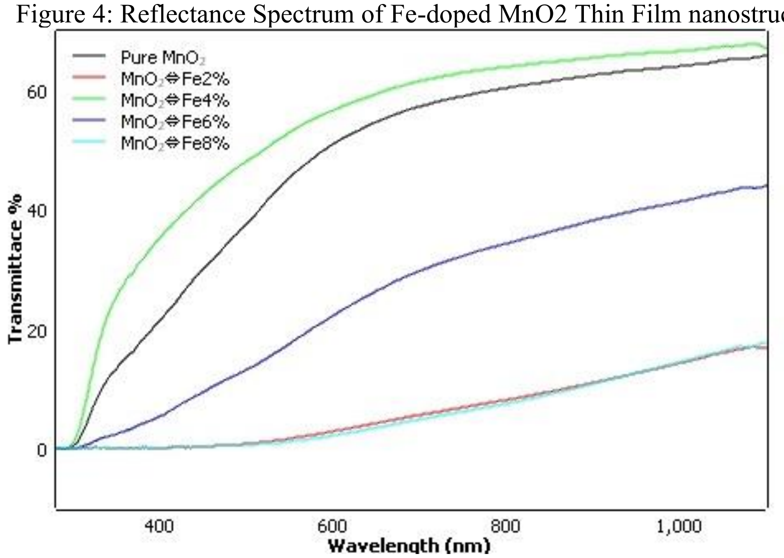

Figure 5: Transmittance Spectrum of Fe-doped Thin Film Nanoparticles

Figure 5 display the transparency capacity of the thin film nanostructures and a maximal transparency of 67.23% was observed. This shows the materials are not shapely transparent and does not glows.

The Tauc's plot as seen by Al-Nidawi, Matori, Zakaria and Zaid (2017) was deployed in other to determine the energy band gap of the nanostructures

$$(\alpha h v)^2 = A(hv - E_g) \quad (6)$$

A is the absorption coefficient calculated as $2.303A/f$ where A is the experimental absorption data and *f* is the thickness of the thin film nanostructures, h represents the plank's constant, hv is the energy obtained from the solar radiation given as $E = 1240/\lambda$ in Zahan and Jiban (2020) and Eg is the band gap of the materials. In other to determine the energy band gap of the nanostructures, $(\alpha h\nu)^2$ was plotted against hν, by setting $(\alpha h\nu)^2$ equals to zero the energy band gag was obtained as shown in figure 6 Table 3 shows the optical properties of the thin film nanoparticle, the energy ban gab of the thin film was observed to be at the range of 1.76 to 3.37ev. The energy gap decreased from 4% doping concentration of Fe, after a significant increase from 0% doping concentration, and the effect observed on the band gap of MnO_2 was due to the metallic ions of Fe present in the nanostructures.

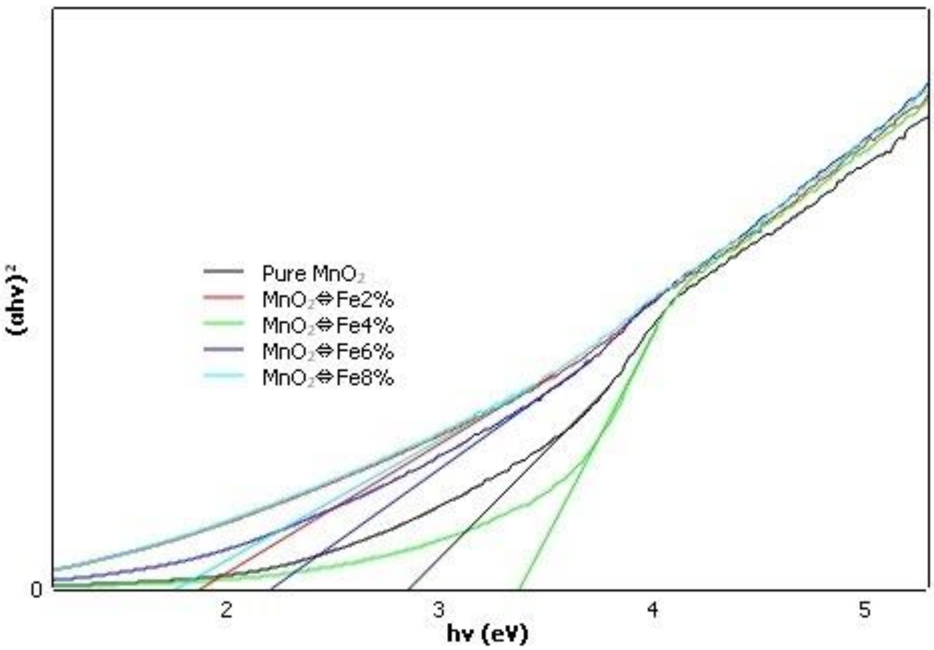

Figure 6: Tauc's Plot Fe-doped MnO_2 Thin Film nanostructures

Table 3: The Optical properties of Fe-Doped MnO_2 Thin Film Nanostructures

Thin Film	Absorbance (%)	Transmittance (%)	Eg (eV)
Pure MnO_2	91.7	65.35	2.86
MnO_2 ⇔ Fe2%	94.91	17.13	1.88
MnO_2 ⇔ Fe4%	93.63	67.75	3.37
MnO_2 ⇔ Fe6%	95.02	44.43	2.21
MnO_2 ⇔ Fe8%	93.36	18.24	1.76

FTIR Analysis

The chemical bond of the thin film nanostructure was determined using the Fourier Transform Infrared Ray spectroscopy as shown in figure 4. The analysis was obtained at transmission spectrum ranging from 600 to 4000cm^{-1}. The FTIR result shows a significant impact of Fe on MnO_2 nanostructure as observed in figure 8 at peak value of 762.3, 890.3 and 2094cm^{-1}. Peak values of 762.3 and 890.3cm^{-1} indicate the blue print vibrations of the thin film nanostructures and 2094cm^{-1} peak value signify string C-H stretching vibrations.

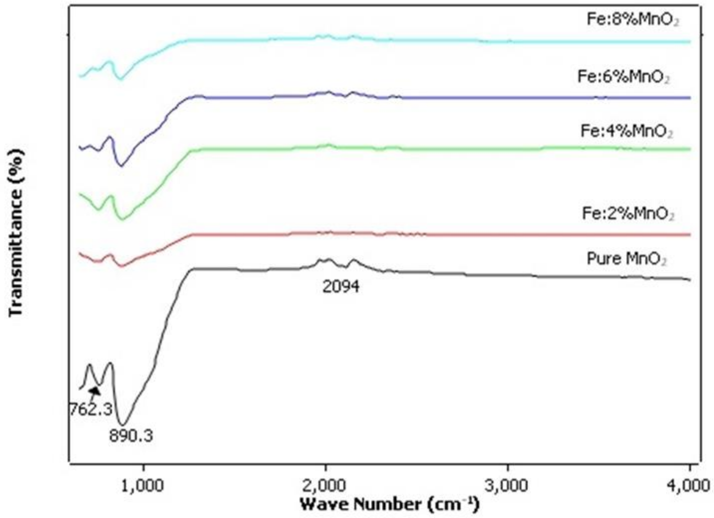

Figure 7: FTIR Spectrum for Fe-doped MnO_2 Thin Film

Electrical Analysis of Fe-doped MnO_2 Thin Film

The Hall Effect characterization was used to determine the electrical properties of the thin film nanoparticles at 0.5µm thickness and 0.1µA, this was used to determine the resistivity, conductivity, mobility and the bulk concentration of the thin film nanostructures annealed at 300K as show in Table 3. The resistivity of the thin film was significantly affected by the doping concentration Fe ions, which shows a remarkable improved electrical property of the Fe-doped MnO_2.

Table 4: Electrical Properties of Fe-doped MnO_2 Thin Films

Thin Films	Resistivity $x10^4$ (Ωcm)	Conductivity $x10^{-4}$ $(\Omega cm)^{-1}$	Mobility (cm^2/Vs) $x10^3$	Bulk Concentration $x10^{11}(cm)^{-3}$
Pure MnO_2	1.719	0.582	5.265	-0.069
MnO_2 ⇔ Fe2%	0.493	2.027	1.868	-6.771
MnO_2 ⇔ Fe4%	2.897	3.452	0.928	-0.232
MnO_2 ⇔ Fe6%	2.911	3.435	0.326	-6.587
MnO_2 ⇔ Fe8%	3.039	3.290	0.218	-9.434

The effect of the Fe-doping concentration spread across the mobility, and conductivity of the thin film show a unique properties to what is obtainable in many literatures, which makes this nanostructure more efficient for sola application.

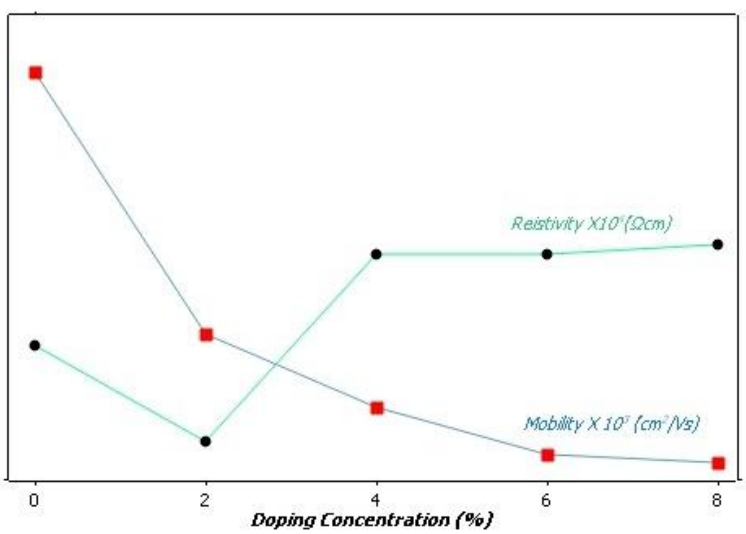

Figure 8: Comparing of Resistivity and Mobility with Doping Concentration

CONCLUSION

The structural, optical, chemical composition and electrical properties of Fe-doped MnO_2 thin film nanostructures prepared by spray pyrolysis deposition method were determined. The structural properties of the thin film was obtained at 2θ ranging between 3-70^0, the XRD peaks was observed at 100, 002, 101, 102, 110, 103 and 112 crystallographic plane at 2θ = 32.02^0, 34.67^0, 36.47^0, 47.8^0, 56.92^0, 62.94^0 and 67.95^0 respectively. It was also observed that the peaks match with each other with acuteness, the sharpness of the peaks confirms the crystal nature of the nanostructures. The crystalline size D (nm) of the thin film at 0, 2, 4, 6, and 8% doping concentration of Fe was found to be 22, 9, 25, 28 and 10nm respectively as shown in Table 2.0, the Williams-Hall Plot analysis was used to obtain the tensile strain of the particles by using a linear fitting plot, and MnO2 ⇔ Fe 2% thin film shows a compression strain of – 0.7720. The optical properties of the thin film was determined using UV-Vis spectroscopy at wavelength between 190-1200nm, the UV analysis gives the transmittance, absorbance and reflectance level of the nanostructures, the nanoparticles transparency of the thin film wasn't sharp but instead it was translucent, but its absorbance was optimal. The Tauc's plot was used to obtain the energy band gab of the thin film, it was founded to be between 1.76-3.37eV, and this band gab is good as regarding to the absorption layer of solar cells. The chemical bond of the thin film nanostructure was determined using the Fourier Transform Infrared Ray spectroscopy. The analysis was obtained at transmission spectrum ranging from 600 to 4000cm^{-1}. The FTIR result shows a significant impact of Fe on MnO_2 nanostructure as observed in figure 7. at peak value of 762.3, 890.3 and 2094cm^{-1}. Peak values of 762.3 and 890.3 indicate the blue print vibrations of the thin film nanostructures and 2094cm^{-1} peak value signify string C-H stretching vibrations. The Hall Effect characterization was used to determine the electrical properties of the thin film, where the resistivity, conductivity, mobility and bulk concentrations of the thin film was obtained. The resistivity value of the thin film was found at 10^4Ωcm, which is lower to what was presented in the literatures, this value has shown a significant improvement of the MnO_2 nanostructures as a result of Fe doping concentration which directly affect its conductance and mobility. The result indicates that the Fe-doped MnO_2 thin films will play a vital role in the fabrication of device including the absorption layer of solar cells.

ACKNOWLEDGEMENT

We acknowledge the Physics department at First Technical University Ibadan for providing us with the required essential apparatus for this research. And also, Advanced Physics Lab at SHESTCO for the use of laboratory facilities.

REFERENCES

Al-Nidawi A. J. A, Matori K. A, Zakaria A and Mohd Zaid, "Effect of MnO2 doped on physical, structure and optical properties of zinc silicate glasses from waste rice husk ash," *ScienceDirect,* vol. 7, pp. 955-961, 2017.

Clark J and Marsden S. R., "Chemistry of Iron," *LibreTexts,* 2024.

Dakhel A, "Structural and electrical properties of Zn doped Mn oxide thin films grown on p-Si substrates," *ScienceDirect,* vol. 454, no. 1-2, pp. 24-30, 2008.

Gokon N, Nishizawa A, Yawata T, Bellan S, Kodama T, and Cho H.-S. "Fe-doped manganese oxide redox material for thermochemical energy storage at high-temperatures," in *AIP Conference Proceedings*, Japan, 2019.

Hastuti A, Subhan A, Amonpattaratkit P, Zainuria M, and Suasmoro S. "The effects of Fe-doping on MnO2: phase transitions, defect structures and its influence on electrical properties," *Royal Society of Chemistry,* p. 7808–7823, 2021.

Hazaa S. K. "The Determination of Optical Band and Optical Constants of MnO2 Thin Films Prepared by Spray Pyrolysis," *UAD Journal of Management Systems,* vol. 5, 2013.

Julien C. M and Mauger A. "Nanostructured MnO2 as Electrode Materials for Energy Storage," *MDPI,* no. 11, 2017.

Khan A., Mohammad A., Mohammad A. T., Tariq F., Khan Y., Hussain R., Aktar N and Rahamn S. U. "Influence of Fe doping on the structural, optical and thermal properties of α-MnO2 nanowires," *IOP Science,* 2019.

Levish A. Joshi S. and Winterer M. "Chemical vapor synthesis of nanocrystalline iron oxides," *ScienceDirect,* 2023.

Liang Z, Chen Z , Xu Y, Wang H, Zhou L and Yan B, "Sustainable production of Fe-doped MnO2 nanoparticles for accelerated tetracycline antibiotic detoxification," *SienceDirect,* vol. 344, 2023

Liu S, Huan H. Yang C, Liu Y, . Li H, Xia H, . Qin T, Zhou I and Liu X, "Electrochemical activation enabling structure reconstruction of Fe-doped MnO2 for enhancing pseudocapacitive storage," *ScienceDirec,* vol. 441, 2022.

Mane R. S.and Lokha A. V.nde C. D., "Chemical deposition method for metal chalcogenide thin films," *Elsevier,* pp. 1-31, 2000.

Nassiri C, Hadri A, Chafi F, Hat A. E, Hassanain N, Rouchdi M., Fares B. and Mzerd A., "Structural, Optical and Electrical Properties of Fe Doped SnO2 Prepared by Spray Pyrolysis," *Journal of materials and Environmental Sciences,* vol. 8, no. 2, pp. 420-425, 2017.

Patrice R., Dupont L., Jumas J. C., Wang E. and Tarascon J. M. "Structural and Electrochemical Properties of Newly Synthesized Fe-Substituted MnO2 Samples," *ACS Publications,* vol. 14, pp. 2772-2782, 2004.

Radhamani A. V., M. . K. Surendra and R. S. Rao, "Zn doped δ-MnO nano flakes: An efficient electrode material for aqueous and solid state asymmetric supercapacitors," *ScienceDirect,* vol. 450, pp. 209-218, 2018.

Salehl A. M. "Improvement of the Optical Properties of Zn-Doped MnO Nanocomposites Thin Fimls," *Passer Journal,* no. 2, pp. 348-355, 2023.

Sasikala, S. Varshaa and V. Kalaiselvi, "Synthesis and Characterization of Fe-doped Manganese Oxide Nanoparticle by using Chemical Precipitation Method," *Journal of Environmental Nanotechnology,* vol. 9, pp. 8-11, 2020.

Silver J. The Chemistry of Iron, Essex UK: Springer Dordrencht, 1993.

Song L., Duan Y., Cui Y. and Huang Z. "Fe-Doped MnO Nanostructures for Attenuation–Impedance Balance-Boosted Microwave Absorption," *ACS Publications,* vol. 5, pp. 2738-2747, 2022.

Soonmin H. "Recent Advances in the Growth and Characterizations of SILAR-Deposited Thin Films," *Applied Science,* 2022.

Thiagarajan S, Sanmugam A. and Vikraman . D. "Facile Methodology of Sol-Gel Synthesis for Metal Oxide Nanostructures," *OPEN ACCESS PEER-REVIEWED CHAPTER,* 22 March 2017.

Umar M, Swinkels M, De Luca M, Fasolato C, Moser L, Díez G, Marot L. Glatzel T, Zardo, I. “Morphological and Stoichiometric Optimization of Cu2O Thin Films by Deposition Conditions and Post-Growth Annealing” Thin Solid Films 732, 138763, 2021

Vijaykumar B. T, Manjunatha and B. Sannakki, "Studies on Structural, Morphological, Electrical, and Gas Sensing Properties of the Polyaniline/Manganese Dioxide (PANI/MnO2) Composites," *Indian Journal of Science and Technology,* vol. 17, no. 32, pp. 3361-3367, 2024.

Yadav V. Shukla R and Sharma K. S. "Impact of Zn-doped Manganese Oxide Nanoparticles on Structural and Optical Properties, *Journal Of Scientific Research,* vol. 14, pp. 867-876, 2022.

Zahan M. and Jiban P. "Structural, optical and electrical properties of Cu:MnO2 nanostructured thin films for glucose sensitivity measurements," *Springer Nature Link,* vol. 2, 2020.